

## Article

# High Reactivity of Dimethyl Ether Activated by Zeolite Ferrierite within a Fer Cage: A Prediction Study

Xiaofang Chen <sup>1,2,\*</sup> , Pei Feng <sup>2</sup>  and Xiujie Li <sup>3,\*</sup> 

<sup>1</sup> Institute of Frontier Chemistry, School of Chemistry and Chemical Engineering, Shandong University, Qingdao 266237, China

<sup>2</sup> State Key Laboratory of Molecular Reaction Dynamics, Dalian Institute of Chemical Physics, Chinese Academy of Sciences, Dalian 116023, China; fengpei@stdu.edu.cn

<sup>3</sup> State Key Laboratory of Catalysis, Dalian Institute of Chemical Physics, Chinese Academy of Sciences, Dalian 116023, China

\* Correspondence: xf.chen@sdu.edu.cn or chen\_smiling@163.com (X.C.); xiujieli@dicp.ac.cn (X.L.)

**Abstract:** The zeolite-catalyzed conversion of DME into chemicals is considered environmentally friendly in industry. The periodic density functional theory, statistical thermodynamics, and the transition state theory are used to study some possible parallel reactions about the hydrogen-bonded DME over zeolite ferrierite. The following are the key findings: (1) the charge separation probably leads to the conversion of a hydrogen-bonded DME into a dimethyl oxonium ion (i.e., DMO<sup>+</sup> or (CH<sub>3</sub>)<sub>2</sub>OH<sup>+</sup>) with a positive charge of about 0.804 e; (2) the methylation of DME, CH<sub>3</sub>OH, H<sub>2</sub>O, and CO by DMO<sup>+</sup> at the T2O6 site of zeolite ferrierite shows the different activated internal energy ( $\Delta E^\ddagger$ ) ranging from 18.47 to 30.06 kcal/mol, implying the strong methylation ability of DMO<sup>+</sup>; (3) H-abstraction by DMO<sup>+</sup> is about 3.94–15.53 or 6.57–18.16 kcal/mol higher than DMO<sup>+</sup> methylation in the activation internal energy; (4) six DMO<sup>+</sup>-mediated reactions are more likely to occur due to the lower barriers, compared to the experimental barrier (i.e., 39.87 kcal/mol) for methyl acetate synthesis; (5) active intermediates, such as (CH<sub>3</sub>)<sub>3</sub>O<sup>+</sup>, (CH<sub>3</sub>)<sub>2</sub>OH<sup>+</sup>, CH<sub>3</sub>CO<sup>+</sup>, CH<sub>3</sub>OH<sub>2</sub><sup>+</sup>, and CH<sub>2</sub>=OH<sup>+</sup>, are expected to appear; (6) DMO<sup>+</sup> is slightly weaker than the well-known surface methoxy species (ZO-CH<sub>3</sub>) in methylation; and (7) the methylated activity declines in the order of DME, CH<sub>3</sub>OH, H<sub>2</sub>O, and CO, with corresponding rate constants at 463.15 K of about  $3.4 \times 10^4$ ,  $1.1 \times 10^2$ , 0.18, and  $8.2 \times 10^{-2} \text{ s}^{-1}$ , respectively.

**Keywords:** zeolite; dimethyl ether; carbonylation; ferrierite; oxonium ion; periodic density functional theory (PDFT); periodic boundary structure; barrier; rate constant



**Citation:** Chen, X.; Feng, P.; Li, X. High Reactivity of Dimethyl Ether Activated by Zeolite Ferrierite within a Fer Cage: A Prediction Study. *Molecules* **2024**, *29*, 2000. <https://doi.org/10.3390/molecules29092000>

Academic Editors: Athanassios C. Tsipis, Feng Xu and Baoyu Liu

Received: 4 March 2024

Revised: 14 April 2024

Accepted: 15 April 2024

Published: 26 April 2024



**Copyright:** © 2024 by the authors. Licensee MDPI, Basel, Switzerland. This article is an open access article distributed under the terms and conditions of the Creative Commons Attribution (CC BY) license (<https://creativecommons.org/licenses/by/4.0/>).

## 1. Introduction

Acidic zeolites have been widely used to catalyze the conversion of dimethyl ether (DME) or methanol into valuable chemicals (e.g., olefins, methyl acids, and methyl acetates (MAs)) over the past several decades. In 2006–2007, the Iglesia group [1–3] reported that acidic zeolites like mordenite and ferrierite, which serve as halide-free catalysts, have the ability to accelerate DME carbonylation. They found that the selectivity towards methyl acetate was particularly high, exceeding 99% at optimized experiment temperatures ranging from 423 K to 463 K. The enduring catalytic activity of those zeolites could be retained for a long time with the progress of chemical reactions, and there is less coke formation during DME carbonylation [1–5]. The outstanding catalytic performances and high product selectivity have received increasing attention in the field of both academy and industry [6–24].

The crystal structures of zeolites are of importance. Zeolite ferrierite is the rare aluminosilicate mineral [25]. In terms of X-ray powder data, the crystalline ferrierite was previously identified as the porous material with the space group of Immm and two obvious intersecting channels [26–28]. The high symmetry of the space group reduces the number

of structural non-equivalent atoms, with one unit cell (UC) of pure-silica FER framework containing eight non-equivalent oxygen atoms and four non-equivalent tetrahedral (T) atoms. Later, the crystal structure of ferrierite was re-determined by the synchrotron X-ray and the neutron powder diffraction experiment, in which the Si-O-Si angle was proved to be  $\sim 170^\circ$  rather than  $180^\circ$  [29]. The favored Al substitution sites were suggested to be at the T2 or T4 site of the acidic zeolite ferrierite [30–32]. Two Brønsted acid (BA) protons at O4 (shared by T1 and T3 cations, pointing to a fer cage) and O6 (shared by two T4 cations) sites of the low-silica ferrierite were recognized by the neutron experiment [33].

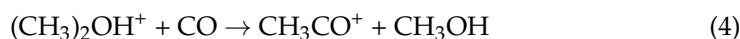
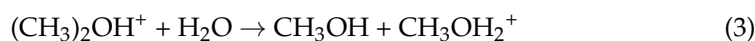
The catalytic behavior of zeolites is nearly determined by the confinement environment around zeolitic Brønsted acid sites, including factors such as the adsorption location, the proton distribution and siting, the acid strength, and the reaction center [11,12,34–39]. Low or undetectable amounts of carbonylation species were evidenced in experiments where certain zeolites lacked eight-membered ring (8MR) channels (e.g., H-BEA, H-FAU, and H-MFI) [1–3]. The eight-member ring channels in zeolites mordenite and ferrierite were suggested as the specific zones for CO insertion into chemisorbed species during DME carbonylation [3,6,7,13,32,40,41]. The shift in hydroxyl vibrational frequency indicated that CO, N<sub>2</sub>, and H<sub>2</sub> preferred a 10-membered ring channel over a fer cage of zeolite ferrierite [42]. Additionally, the interaction of CO with silanol groups was also evidenced at low temperatures, with the carbonyl adsorbed species varying with the temperature [43]. At the reaction temperature, CO and DME molecules assumedly preferred the 8-membered ring channel of zeolite ferrierite [12]. It was found that smaller alkanes than n-pentane could access the entire pore of ferrierite, while longer alkanes preferred the 10-membered ring to the 8-membered ring cage [44]. T2O6 configuration was suggested to be the strongest BA site of the acidic zeolite ferrierite from the statistical perspective [13]. Experimental and theoretical evidence indicated that small molecules like methanol and DME were mainly accumulated in the 8- and 6-member ring channels of zeolite ferrierite [1–3,6,13,32,40].

Based on the potential active intermediate, many researchers have attempted to interpret the fast kinetic process of DME carbonylation. The Iglesia group [1–3] proposed that the surface methoxy species (i.e., SMS or ZO-CH<sub>3</sub>) was a key intermediate with high activity, which served as a catalyst to trigger and propagate the elemental chemical reactions during DME carbonylation. They also presented a potential catalytic circle grounded on ZO-CH<sub>3</sub>. The high reactivity of ZO-CH<sub>3</sub> was theoretically confirmed by other researchers [6,7,13]. Apart from ZO-CH<sub>3</sub>, three species of CH<sub>3</sub>CO<sup>+</sup>, CH<sub>3</sub>OH, and H<sub>2</sub>O were also suggested to be other possible intermediates by the Iglesia group [1–3,16]. Later, Jensen's group [45] theoretically predicted ketene (CH<sub>2</sub>CO) as a possible reaction intermediate for DME carbonylation, and they further verified the existence of ketene by doubly deuterated acetic acid (CH<sub>2</sub>D<sub>2</sub>COOD) in the experiment. Meanwhile, the hydrogen-bonded DME could coexist with ZO-CH<sub>3</sub>, which is frequently detected by the IR spectra experiment with the peaks at 3011, 2971, 2947, and 2844 cm<sup>-1</sup> [1,2,46]. This hydrogen-bonded DME was initially formed by DME reacting with the proton (H<sup>+</sup>) of the acidic zeolite; sometimes, it was regarded as the protonated DME or DME adsorption at the Brønsted acid site [1–3]. The BA proton has a strong tendency to draw the electron density of the electron-rich O atom and then changes the electrostatic potential of the molecule of DME. DME moiety in the adsorption complex is readily activated by acidic zeolite. Even now, it is a relatively unexplored area of research on the chemical role of the hydrogen-bonded DME over the acidic zeolites.

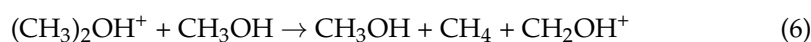
In this study, we design six possible chemical reactions (Equations (1)–(6)) between the attacking molecules and the hydrogen-bonded DME at the T2O6 site of zeolite ferrierite. The attacking molecules are two feed molecules (i.e., DME and CO) and two key intermediates (i.e., CH<sub>3</sub>OH and H<sub>2</sub>O) from DME carbonylation. Equations (1)–(4) are the hydrogen-bonded DME methylating with four attacking molecules (i.e., DME, CH<sub>3</sub>OH, H<sub>2</sub>O and CO), respectively. Equation (5) or (6) is the hydrogen-bonded DME abstracting one of the methyl H atoms of DME or CH<sub>3</sub>OH. Zeolite ferrierite is a porous material with a three-dimensional network topology. We employ the period density functional theory

(PDFT), statistical thermodynamics, and transition state theory to predict the chemical kinetics and the reaction mechanism of those six chemical reactions. The aim of this study is to provide some theoretical evidence to identify the hydrogen-bonded DME as the highly active intermediate from different perspectives.

a. Methylation of hydrogen-bonded DME within the deprotonated zeolite ( $ZO^-$ ):



b. H-abstraction of hydrogen-bonded DME within  $ZO^-$ :



## 2. Results and Discussion

The acidic zeolite ferrierite features an FER framework containing eight non-equivalent oxygen atoms and four non-equivalent tetrahedral (T) atoms in one unit cell [26–28]. The T2O6 site was identified as the strongest acid site of the acidic zeolite ferrierite from a statistical perspective [11]. In this context, we focus on the reactivity of the hydrogen-bonded DME only at the T2O6 site of the acidic zeolite ferrierite. One of the attacking molecules and one DME molecule are all put in the fer cage of the acidic zeolite ferrierite. The attacking molecules influence on the reactivity of  $DMO^+$  at the T2O6 site will be addressed and discussed in the following sections.

### 2.1. DME Adsorbed on the Zeolitic Surface

The experiment observed that DME pressure (0.8–8.0 kPa) did not determine the rate of methyl acetate synthesis [1,2] from DME carbonylation. This phenomenon was likely caused by the active sites saturated by DME-derived intermediates. The Brønsted acid proton is electron-deficient, while the O atom of DME has a lone electron pair. It is generally accepted that DME is first adsorbed end-on at the zeolitic Brønsted acid site via the hydrogen bond interaction. The 8MR channel as the specific zone of DME carbonylation was frequently emphasized in previous studies [3,6,13,32,40,41]. DME adsorbed at the T2O6 site would act as an ion-pair complex [47]. DME could be accumulated in the 8MR channel of the acidic zeolite ferrierite (H-FER). In the adsorption complex, DME is nearly parallel to Figure 1a or perpendicular to Figure 1b, the [010] plane of H-FER. As for the internal energy, the former lies above the latter by 3.25 kcal/mol. The pore size of the 8MR channel in zeolite ferrierite is  $4.8 \times 3.5 \text{ \AA}$  [28], while the molecule size of DME is generally regarded as 4.3–5.0 Å (Figure S1 in Supplementary Materials). When a DME molecule is perpendicular to the [010] plane, it would be better to overcome the space hindrance. This might contribute to accounting for the space preference of DME moiety in the adsorption complex. We only consider DME perpendicular to the [010] plane of H-FER in DME adsorption in the following sections. The Brønsted acid H atom is calculated to be 0.98 Å away from the zeolitic framework O6 atom of the undisturbed H-FER. The BA hydroxyl bond length is elongated to 1.12 Å in the presence of DME. The electron density transfers to the O6 atom from the Brønsted acid H atom, making the  $H \cdots O(CH_3)_2$  moiety exhibit the positive charge, and the Bader charge analysis indicates that  $H \cdots O(CH_3)_2$  moiety has the positive charge of about 0.804 e. The moiety of  $H \cdots O(CH_3)_2$  in the adsorption complex tends to become a somewhat dimethyl oxonium ion [48] (i.e.,  $(CH_3)_2OH^+$  or  $DMO^+$ ) via the charge separation. For convenience,  $DMO^+$  is used to represent the hydrogen-bonded DME in the following sections.

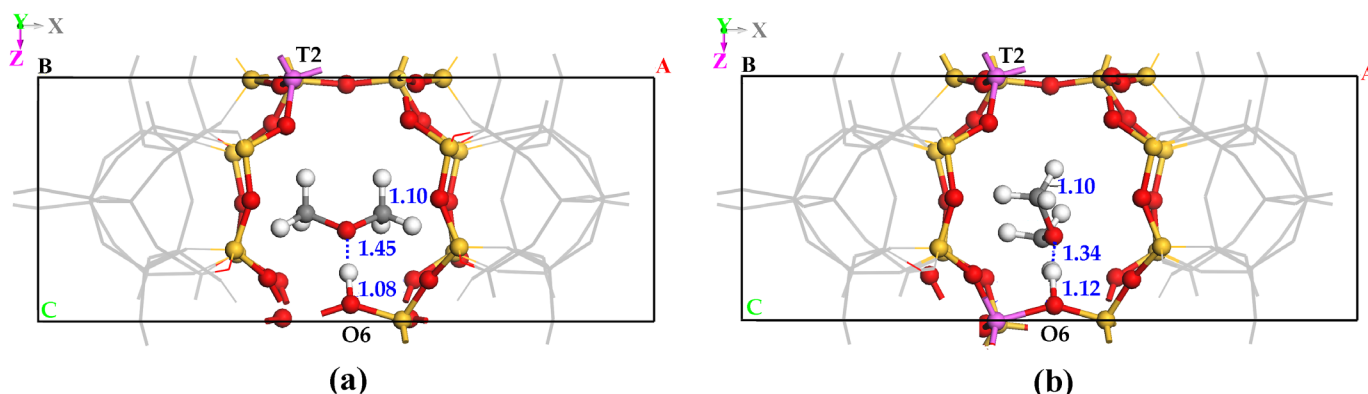


**Figure 1.** Dimethyl ester (DME) adsorbed at the T2O6 site of zeolite ferrierite within the eight-membered ring (8MR) channel: (a) parallel to and (b) perpendicular to the [010] plane. Noting that (1) O in red, Si in yellow, Al in pink, C in grey, and H in white; (2) grey lines for interconnecting atoms away from the 8MR, and (3) the blue number is the distance (in Å) between two atoms.

## 2.2. Attacking Molecule Serving as Electron Donor

In the context of DME carbonylation, DME and CO serve as main feed materials, while  $\text{CH}_3\text{OH}$  and  $\text{H}_2\text{O}$  are suggested to be two key intermediates of DME carbonylation [1,2,13]. Each molecule of DME,  $\text{CH}_3\text{OH}$ , or  $\text{H}_2\text{O}$  has two lone electrons stationed at the O atom (Scheme 1a). A CO molecule has a triple covalent  $\text{C}\equiv\text{O}$  bond originating from three pairs of shared double electrons: two pairs are from C and O atoms, while the third pair is completely from the O atom and then enters an unoccupied  $p$ -orbital of the C atom (Scheme 1b). Those four molecules all have the lone electron pair. DME,  $\text{CH}_3\text{OH}$ ,  $\text{H}_2\text{O}$ , or CO belongs to the electron-rich molecule. Consequently, each molecule is expected to have the ability to act as an electron donor.



**Scheme 1.** Lone electrons in (a) DME,  $\text{CH}_3\text{OH}$ , and  $\text{H}_2\text{O}$ , and (b) CO. Notes: (1) for DME,  $\text{R1} = \text{R2} = -\text{CH}_3$ ; (2) for  $\text{CH}_3\text{OH}$ ,  $\text{R1} = \text{CH}_3$ ,  $\text{R2} = \text{H}$ ; (3) for  $\text{H}_2\text{O}$ ,  $\text{R1} = \text{R2} = \text{H}$ ; (4) a red or black dot represents an electron from the O or C atom.

## 2.3. Methylation Process of Hydrogen-Bonded DME (i.e., $\text{DMO}^+$ )

### 2.3.1. Reaction Course of $\text{DMO}^+$ Methylation

DME,  $\text{CH}_3\text{OH}$ ,  $\text{H}_2\text{O}$ , and CO are assumedly abundant in DME carbonylation. The O atom of DME,  $\text{CH}_3\text{OH}$ , or  $\text{H}_2\text{O}$  and the C atom of CO are defined as the target A atom in this study. When DME is adsorbed at the T2O6 site of the acidic zeolite ferrierite in the presence of an attacking molecule ( $\text{R1-O-R2}$ ), we could put an attacking molecule into a fer cage along the eight-membered ring channel of the acidic zeolite ferrierite (Figure 2). As shown in Figure 2, the target A atom would be most close to one of the methyl groups of the hydrogen-bonded DME. In the reactant systems of Re1-Re4, the BA hydroxyl bond length ( $d(\text{O6-Hz})$ ) is stretched to 1.31, 1.28, 1.28, and 1.15 Å, respectively, already elongated relative to that (0.98 Å) in the undisturbed H-FER. Meanwhile, the BA proton further approaches the O atom of DME, and the moiety of  $\text{H}\cdots\text{O}(\text{CH}_3)_2$  is with the larger positive charge. The Bader charge analysis indicates that the charge of  $\text{H}\cdots\text{O}(\text{CH}_3)_2$  moiety in Re1-Re4 is about 0.790 e, 0.919 e, 0.945 e and 0.739 e, respectively. In turn, the transmethylation could occur between the electron-deficient  $\text{DMO}^+$  and the electron-rich attacking molecule via the  $\text{S}_\text{N}2$ -like [49] transition state (i.e., TS1-TS4) (Figure 2), in which three atoms,  $\text{O}_\text{D}$ ,  $\text{C}_\text{M}$ , and

target A atom in each transition state, are almost in line with the  $\angle O_D C_M A$  angle ranging from  $168.85^\circ$  to  $178.54^\circ$ . Herein,  $H_Z$ ,  $C_M$ ,  $O_D$ , and A are the BA proton, the migrant C atom, the O atom of the activated DME, and the target A atom. The migrant methyl group becomes nearly planar ( $\angle C_M H H H$  below  $7.86^\circ$ ) from the umbrella undisturbed  $DMO^+$ . For the structures and the coordinates of reactants and transition states, please refer to Supplementary Materials.

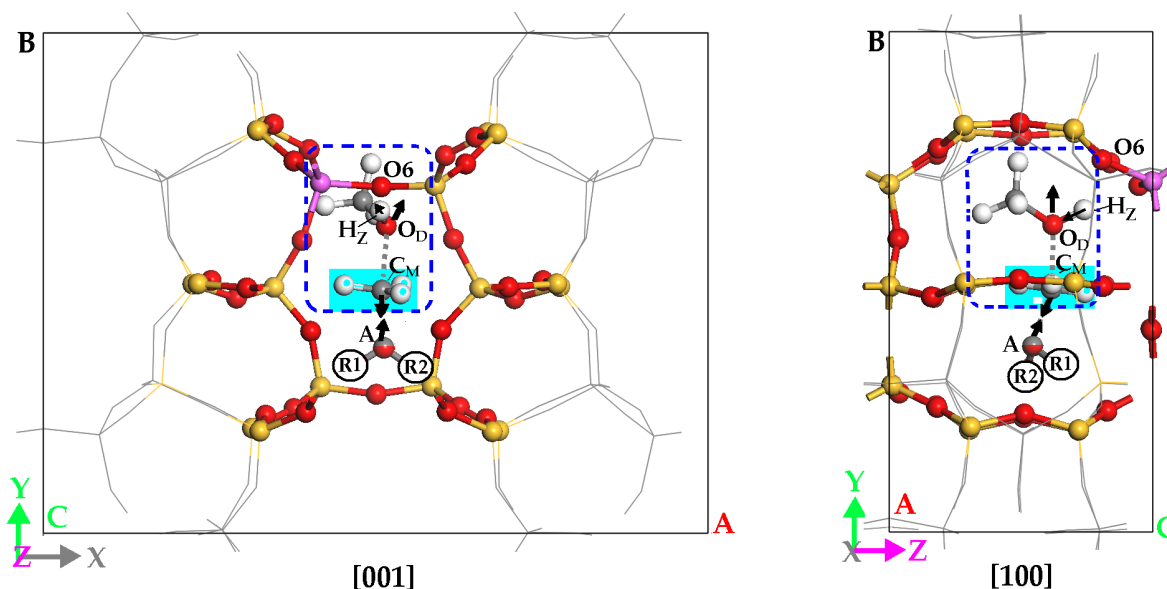


**Figure 2.** Within a fer cage of zeolite ferrierite, an attacking molecule (R1-A-R2) is methylated by a hydrogen-bonded DME molecule (i.e.,  $DMO^+$ ) at the T2O6 site (in a blue dash square). Notes: (1) O in red, Si in yellow, Al in pink, C in grey, and H in white, and grey lines for interconnecting atoms and bonds away from the fer cage; (2) DME: A = O, R1 = R2 = CH<sub>3</sub>; (3) CH<sub>3</sub>OH: A = O, R1 = CH<sub>3</sub>, R2 = H; (4) H<sub>2</sub>O: A = O, R1 = R2 = H; (5) CO: A = C, R1 = O, and R2 is omitted; (6)  $H_Z$ ,  $O_D$ ,  $C_M$ , and A are the Brønsted acid proton, O atom of DME, the migrant C atom, and target A atom, and (7) the black arrow is the main direction of atom movement.

The calculated imaginary frequency is  $398.94i$ ,  $389.71i$ ,  $381.85i$ , or  $542.61i$ , responsible for the bond breakage and the bond formation when  $DMO^+$  methylating with DME, CH<sub>3</sub>OH, H<sub>2</sub>O, or CO. The black arrows in Figure 2 show the direction of atom movement of interest. As shown, the will-be-broken chemical bonds involve the BA hydroxyl bond (i.e., O6- $H_Z$ ) of H-FER and the C-O bond of DME, while two new bonds would be formed between (i) the acidic zeolite BA proton and the O atom of DME, and (ii) between the migrant methyl group of the hydrogen-bonded DME and target A atom of the attacking molecule (R1-A-R2). Along the reaction course of  $DMO^+$  methylation, the BA proton gradually moves away from the zeolitic framework O6 atom and scrambles to the O atom of DME; the migrant methyl group ( $-C_M H_3$ ) gradually scrambles to the target atom (A) of the attacking molecule.

Figure 3 further shows the numerical change of structure parameters of interest. Along the reaction course of reactant (Rex)  $\rightarrow$  transition state (TSx)  $\rightarrow$  product (Px) (x = 1–4), as calculated, (i) either the BA hydroxyl distance (i.e.,  $d(O6-H_Z)$ ) (Figure 3a) or the distance between the BA proton and O atom of DME moiety (i.e.,  $d(O_D-C_M)$ ) (Figure 3c) generally grows; (ii) either the distance between the BA proton and the O atom of DME (i.e.,  $d(H_Z-O_D)$ ) (Figure 3b) or the distance between the migrant C atom ( $C_M$ ) of  $DMO^+$  and the target atom (A) of the attacking molecule (i.e.,  $d(C_M-A)$ ) (Figure 3d) declines gradually; (iii) three atoms  $O_D$ ,  $C_M$ , and A (Figure 3e), oscillate and their angle (i.e.,  $\angle O_D C_M A$ ) wanders around  $180^\circ$ ; but (iv) the dihedral angle of  $H_Z O C_M A$  (i.e.,  $\angle H_Z O C_M A$ ) changes and yet does not have the same trend. Taking TS4 for an example,  $d(O6-H_Z)$  in TS4 is stretched to  $1.70 \text{ \AA}$

from 1.12 Å in DME adsorption complex (Figure 1b) while  $d(\text{H}_Z\text{-O}_D)$  in TS4 is shrunk to 1.01 Å from 1.34 Å in the DME adsorption complex (Figure 1b);  $d(\text{C}_M\text{-A})$  in TS4 becomes 1.91 Å from 3.76 Å in Re4;  $\angle\text{O}_D\text{C}_M\text{A}$  in TS4 is equal to 168.85°, and  $\angle\text{H}_Z\text{OC}_M\text{A}$  equals to 153.81°.

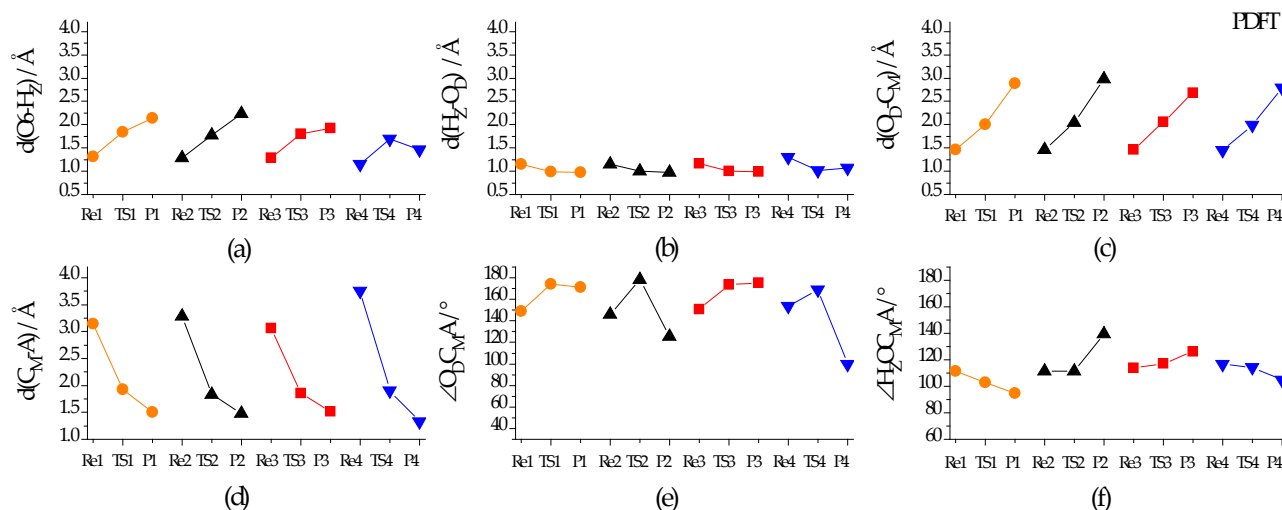


**Figure 3.** Some distances ( $d$ ) and angles ( $\angle$ ) in the reactant (Re $x$ ), the transition state (TS $x$ ), and the product (P $x$ ) of Equation ( $x$ ) ( $x = 1-4$ ) in the Section 1: (a)  $d(\text{O}_6\text{-H}_Z)$ , (b)  $d(\text{H}_Z\text{-O}_D)$ , (c)  $d(\text{O}_D\text{-C}_M)$ , (d)  $d(\text{C}_M\text{-A})$ , (e)  $\angle\text{O}_D\text{C}_M\text{A}$ , and (f)  $\angle\text{H}_Z\text{OC}_M\text{A}$ . Notes: (1)  $\text{O}_6$ ,  $\text{H}_Z$ ,  $\text{O}_D$ , and  $\text{C}_M$  are the framework  $\text{O}_6$  atom and the BA proton of zeolite ferrierite, and the O atom and the migrant C atom of the hydrogen-bonded DME (i.e.,  $\text{DMO}^+$ ); (2) A is the O atom of DME,  $\text{CH}_3\text{OH}$  or  $\text{H}_2\text{O}$  moiety, yet it is the C atom of CO moiety; (3) Each color represents the species in one chemical equation.

### 2.3.2. Energy Parameters and Products for $\text{DMO}^+$ Methylation

Figure 4 shows that the activated internal energies ( $\Delta E^\ddagger$ ) for those four methylation reactions (Equations (1)–(4)) are all below 30.06 kcal/mol when  $\text{DMO}^+$  is located at the T2O6 site, and the attacking molecule is within the fer cage of zeolite ferrierite. This implies that those transmethyations readily proceed rapidly in kinetics. Among the four attacking molecules, the DME molecule needs to overcome the lowest activated internal energy ( $\sim 18.47$  kcal/mol) after adsorbing a lower reaction heat of about 9.39 kcal/mol. In contrast, CO requires surmounting the highest activated internal energy ( $\sim 30.06$  kcal/mol) despite releasing a low reaction heat of approximately  $-8.36$  kcal/mol. Thus, the methylation of DME by  $\text{DMO}^+$  would be kinetically favored, while the methylation of CO by  $\text{DMO}^+$  would be thermodynamically favored at the T2O6 site of zeolite ferrierite. The methylation of DME by  $\text{DMO}^+$  yields a contentious active species called trimethyloxonium ion ( $\text{TMO}^+$  or  $(\text{CH}_3)_3\text{O}^+$ ), which plays a crucial role in the first C-C bond formation in the DME/methanol-to-olefin (DMTO) via the direct mechanism [2,6,13,50–52]. When methylating with CO,  $\text{DMO}^+$  might be regarded as an efficient precursor “seed” of the carbon chain growth for C1 species (Equation (4)), firstly generating  $\text{CH}_3\text{CO}^+$  and then likely leading to  $\text{CH}_3\text{COCH}_3$  [1,2].  $\text{CH}_3\text{OH}$  methylated by  $\text{DMO}^+$  is an ion exchange reaction in which the reactant species are the same as the product species. Its activated internal energy is 22.13 kcal/mol, close to a theoretical  $\Delta E^\ddagger$  (i.e., 19.9 kcal/mol) for  $\text{CH}_3\text{OH}$  methylated by the most stable  $\text{ZO-CH}_3$  on MOR [6].  $\text{DMO}^+$  methylating with  $\text{H}_2\text{O}$  will produce a highly active intermediate of  $\text{CH}_3\text{OH}_2^+$ , called a methoxonium ion (Equation (3)) [53]. The activated internal energy for  $\text{DMO}^+$  methylating with water is about 6.57 kcal/mol less than that for  $\text{DMO}^+$  methylating with CO.  $\text{DMO}^+$  preference of  $\text{H}_2\text{O}$  over CO also contributes to accounting for the experimental phenomenon that a small amount of water inhibits DME carbonylation [1,2]. Apart from CO, DME,  $\text{CH}_3\text{OH}$ , and  $\text{H}_2\text{O}$  methylated by  $\text{DMO}^+$  are all endothermic. The least endothermic methylation process (i.e., 9.39 kcal/mol) is from DME, followed by  $\text{CH}_3\text{OH}$ . The reaction heat would be easily supplied by DME

carbonylation under the specific condition. To complete the methylation process, two attacking molecules of  $\text{CH}_3\text{OH}$  and  $\text{H}_2\text{O}$  require absorbing the higher reaction internal energy (about 14.78 and 17.67 kcal/mol, respectively). The magnitude of activated internal energy also implies that four attacking molecules exhibit differently methylated abilities; in kinetics, the order is assumedly  $\text{DME} > \text{CH}_3\text{OH} > \text{H}_2\text{O} > \text{CO}$ . It is worth noting that the calculated activated internal energies for those four methylation processes are all lower than the deduced experimental barrier (about 39.87 kcal/mol) for methyl acetate synthesis [1,2].

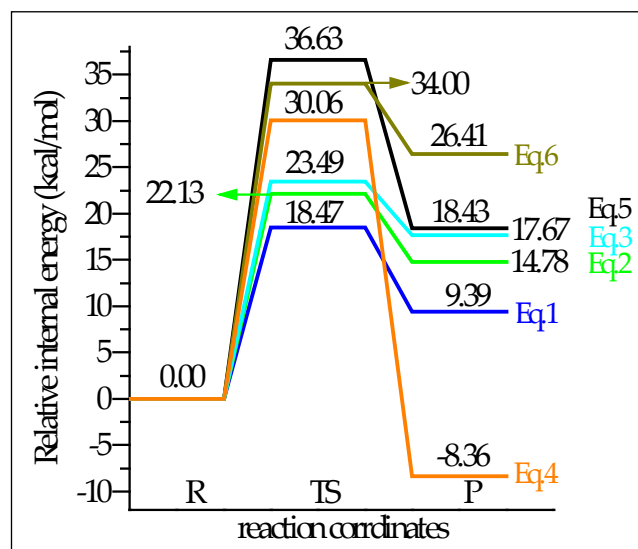


**Figure 4.** Calculated energy profile for  $\text{DMO}^+$  methylation and H-abstraction at T2O6 site of zeolite ferrierite within a fer cage. For Equations (1)–(6), please refer to the Section 1.

#### 2.4. H-Abstract of Hydrogen-Bonded DME (i.e., $\text{DMO}^+$ )

##### 2.4.1. Reaction Course of $\text{DMO}^+$ H-Abstraction

When DME is adsorbed at the T2O6 site, the attacking molecule of DME or  $\text{CH}_3\text{OH}$  is located within a fer cage of the acidic zeolite ferrierite in another manner, where the methyl group of DME or  $\text{CH}_3\text{OH}$ , rather than the O atom, is most close to the migrant methyl group of the activated DME (Figure 5). The Brønsted acid hydroxyl bond length ( $d(\text{O6-Hz})$ ) is calculated to be 1.12 or 1.14 Å in the reactant system of Re5 or Re6 (the structure is similar to that in Figure 5). It is slightly elongated by 0.14 or 0.16 Å relative to the undisturbed H-FER (i.e.,  $d(\text{O6-Hz}) = 0.98$  Å). When the Brønsted acid proton gradually approaches the O atom of DME, the partial electron density will move to the O atom of DME, resulting in the moiety of  $\text{H}\cdots\text{O}(\text{CH}_3)_2$  with the positive charge. The Bader charge analysis indicates that  $\text{H}\cdots\text{O}(\text{CH}_3)_2$  moiety in Re5 or Re6 has a positive charge of about 0.769 e or 0.764 e. This implies that the hydrogen-bonded DME in Re5 or Re6 is already activated by the Brønsted acid proton. The migrant methyl group of the hydrogen-bonded DME (i.e.,  $\text{DMO}^+$ ) exhibits a weak carbenium ion, and the calculated Bader charge is about 0.580 e or 0.575 e. Within the deprotonated zeolite ferrierite, it is expected that the hydrogen-bonded DME (i.e.,  $\text{DMO}^+$ ) will abstract one of the methyl H atoms of DME or  $\text{CH}_3\text{OH}$ .

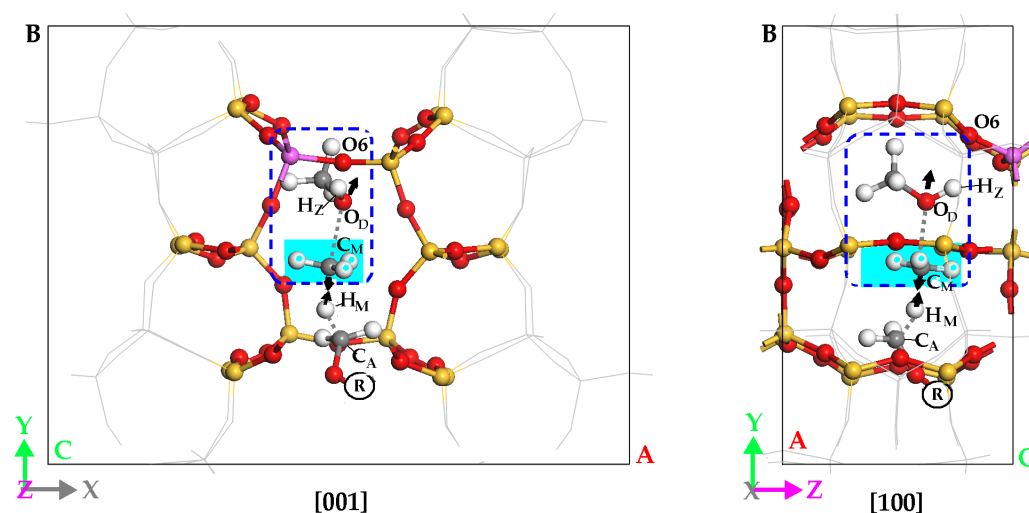


**Figure 5.** The hydrogen-bonded DME (in blue dash square) abstracts one of methyl H atoms of attracting molecules (i.e., DME or  $\text{CH}_3\text{OH}$ ) at the T2O6 site within a fer cage of zeolite ferrierite. Notes: (1) O in red, Si in yellow, Al in pink, C in grey, and H in white, grey lines for interconnecting atoms and bonds away from the fer cage; (2) for DME,  $\text{R} = -\text{CH}_3$ ; for  $\text{CH}_3\text{OH}$ ,  $\text{R} = \text{H}$ ; (3)  $\text{O}_\text{D}$ ,  $\text{C}_\text{M}$ , and  $\text{H}_\text{M}$  are the O atom and the migrant methyl C atom of hydrogen-bonded DME, and the migrant methyl H atom of attracting molecules, and (4) the black arrow is the main direction of atom movement of interest.

Two transition states, TS5 and TS6 are located (the structure is similar to Figure 5), which are responsible for  $\text{DMO}^+$  abstracting the methyl H atom of DME and  $\text{CH}_3\text{OH}$ , respectively. The migrant atoms in transition states are mainly (i) Brønsted acid proton ( $\text{H}_\text{Z}$ ), (ii) the O atom ( $\text{O}_\text{D}$ ) of the hydrogen-bonded DME, (iii) the C atom ( $\text{C}_\text{M}$ ) of the migrant methyl of the hydrogen-bonded DME, (iv) the migrant methyl H atom ( $\text{H}_\text{M}$ ) of DME or  $\text{CH}_3\text{OH}$ , and (v) the C atom ( $\text{C}_\text{A}$ ) of the attacking molecule DME or  $\text{CH}_3\text{OH}$ . For the direction of atom movement of interest, please see the black arrows in Figure 5. Then, the reaction course involves three main parts: the nearly linear  $\text{O6}\cdots\text{H}_\text{Z}\cdots\text{O}_\text{D}$  ( $163.37^\circ$  or  $165.32^\circ$ ), the nearly linear  $\text{O}_\text{D}\cdots\text{C}_\text{M}\cdots\text{H}_\text{M}$  ( $173.76^\circ$  or  $173.37^\circ$ ), and the bent  $\text{C}_\text{M}\cdots\text{H}_\text{M}\cdots\text{C}_\text{A}$  ( $138.61^\circ$  or  $144.24^\circ$ ). The distance ( $d(\text{O6}-\text{H}_\text{Z})$ ) is stretched to 1.82 or 1.77 Å from 0.98 Å in the undisturbed H-FER, implying that the BA proton in TS5 or TS6 is gradually away from the zeolitic surface oxygen. The  $\text{O}_\text{D}\cdots\text{C}_\text{M}$  distance in TS5 or TS6 is stretched to 2.13 Å, then  $\text{DMO}^+$  moiety would undergo the breakage of the  $\text{O}_\text{D}-\text{C}_\text{M}$  bond. The  $\text{H}_\text{M}\cdots\text{C}_\text{A}$  distance in the transition state increases to 1.25 Å from 1.10 Å in the methyl group of DME or  $\text{CH}_3\text{OH}$ , resulting in the breakage of methyl C-H bond of the attacking molecule. The new chemical bond will be formed between the migrant methyl C atom ( $\text{C}_\text{M}$ ) of the reacting  $\text{DMO}^+$  and the methyl H atom of the attacking molecule, and the  $\text{C}_\text{M}\cdots\text{H}_\text{M}$  distance in the transition state is largely shortened to 1.46 Å or 1.40 Å from 3.36 Å or 2.96 Å in the reacting system. The migrant methyl group in TS5 or TS6 is almost in the format of a carbenium ion, and then it becomes nearly planar in order to better interact with the  $\text{O}_\text{D}$  and  $\text{H}_\text{M}$  atoms. For the structural details, refer to Figure S4 and Table S2 in Supplementary Materials.

#### 2.4.2. Energy Parameters and Products for $\text{DMO}^+$ H-Abstraction

When  $\text{DMO}^+$  H-abstraction proceeds, (i) methane ( $\text{CH}_4$ ) would be formed by the nearly planar  $\text{CH}_3^+$  interacting with the methyl H atom, (ii)  $\text{CH}_3\text{OH}$  would be produced by the BA proton transfer and the O-C bond breakage of  $\text{DMO}^+$ , and (iii) the attacking molecule of DME or  $\text{CH}_3\text{OH}$  becomes  $\text{CH}_3\text{OCH}_2^+$  or the protonated formaldehyde ( $\text{CH}_2\text{OH}^+$ ) by losing one of methyl H atoms. Whether the attacking molecule is  $\text{CH}_3\text{OH}$ , the H-abstraction of  $\text{DMO}^+$  within zeolite ferrierite probably undergoes a so-called methane-formaldehyde mechanism, similar to some reactions in methanol-to-olefins [54–56]. The active intermediate  $\text{CH}_3\text{OCH}_2^+$  is capable of being further methylated by the methylating agent, producing

dimethyloxoniummethylide,  $[(\text{CH}_3)_2\text{-O}^+\text{CH}_2^-]$ . This might make DME carbonylation occur via an oxonium ion or oxonium-ylide mechanism, which is frequently mentioned in MTO [48,50,51,57,58]. Our results also indicate that, within a fer cage of zeolite ferrierite, each process of  $\text{DMO}^+$  H-abstraction is endothermic (i.e., 18.43 or 26.41 kcal/mol) and has a moderate activation internal energy of 36.63 or 34.00 kcal/mol. The activation internal energy of  $\text{DMO}^+$  H-abstraction is slightly bigger than that (i.e., 32.32 kcal/mol) for  $\text{ZO-CH}_3$  abstracting the methyl H atom of  $\text{CH}_3\text{OCH}_3$  [54], and yet it is slightly smaller than the deduced barrier (about 39.87 kcal/mol) for methyl acetate synthesis in the experiment [1,2]. This implies that  $\text{DMO}^+$  H-abstraction is more likely to occur within a fer cage of zeolite ferrierite. In terms of the activated internal energy,  $\text{DMO}^+$  H-abstraction is kinetically weaker than  $\text{DMO}^+$  methylation (Section 2.3) or  $\text{ZO-CH}_3$  methylation [2,6,13]. The reason for this is probably because the C-H bond is stronger than the C-O bond. As a result, a very small number of  $\text{CD}_3\text{OCD}_3\text{-CO}$  mixtures were observed in methyl acetate synthesis in the experiment [1,2].

### 2.5. Rate Constant

It is found that DME carbonylation is experimentally carried out at the optimized reaction temperature of 423–463 K [1–5]. At the higher temperature, the entropic effect is an important contribution to the Gibbs free energy. For the micro-heterogeneous catalysis reaction in the elemental step, the reaction belongs to the first-order reaction in terms of transition state theory (TST). The rate constant is related to the Gibbs free energy at a given temperature. The numerical values of the Gibbs free energy could be calculated according to Equations (7)–(11).

$$k = \frac{k_b \cdot T}{h} \exp\left(-\frac{\Delta G(T)^\ddagger}{R \cdot T}\right) \quad (7)$$

$$G(T) = H - T \cdot S \quad (8)$$

$$S = S_e + S_t + S_r + S_v \quad (9)$$

$$S = \left(\frac{\partial F}{\partial T}\right)_{V,N} \quad (10)$$

$$F = -k_b \cdot T \cdot \ln q^N \quad (11)$$

Herein,  $k$  is the first-order rate constant,  $k_b$  is the Boltzmann constant,  $h$  is the Planck constant,  $R$  is the ideal gas constant,  $T$  is the temperature, and  $\Delta G(T)$  is the activation free energy at a given temperature, which could be calculated by the Gibbs free energy ( $G(T)$ ) difference between the transition state and the reactant system.  $G(T)$  is related to the enthalpy ( $H$ ), the temperature ( $T$ ), and the entropy ( $S$ ) (Equation (8)). The entropy ( $S$ ) of the material is the sum of the electric ( $S_e$ ), the transitional ( $S_t$ ), the vibrational ( $S_v$ ), and the rotational ( $S_r$ ) entropy (Equation (9)). The entropy stems from the derivative of Helmholtz free energy ( $F$ ) divided by the temperature at the constant volume and the constant number of particles (Equation (10)). And the Helmholtz free energy ( $F$ ) is related to the partition function ( $q$ ) (Equation (11)). The temperature selected ranges from 273.15 to 773.15 K in this study.

Figure 6 illustrates the rate constants dependent on the temperature. As calculated, the rate constants for  $\text{DMO}^+$  methylating with CO or  $\text{H}_2\text{O}$ , as well as  $\text{DMO}^+$  abstracting the methyl H atom of DME or  $\text{CH}_3\text{OH}$ , are below the deduced rate constant (the black line) for methyl acetate synthesis in the experiment [1,2]. Methylated by  $\text{DMO}^+$ , water completes with CO heavily. As calculated,  $\text{DMO}^+$  assumedly prefers water to CO at low temperatures (about <522.60 K), and  $\text{CH}_3\text{CO}^+$  formation is slower than  $\text{CH}_3\text{OH}_2^+$  formation by about 0–2.38 orders of magnitude. This could quantitatively account for water-inhibiting DME carbonylation at the optimized experiment temperatures of 423–463 K [1,2]. In the presence of attacking molecule DME or  $\text{CH}_3\text{OH}$ ,  $\text{DMO}^+$  H-abstraction is 9.23–8.89 or 6.11–5.90 orders of magnitude slower than the corresponding methylation process at 423.15–463.15 K. This

is in line with the experimental observation of the small amount of  $\text{CD}_3\text{OCD}_3\text{-CO}$  mixtures ( $k_H/k_D = 1.06$ ) appearing in DME carbonylation [2]. When H-abstracted by  $\text{DMO}^+$  at the T2O6 site within a fer cage, DME is slower than  $\text{CH}_3\text{OH}$  by 0.50–0.56 orders of magnitude at 443.15–463.15 K. DME carbonylation tends to produce  $\text{TMO}^+$  intermediate in common features with the methanol-to-hydrocarbon process [50].

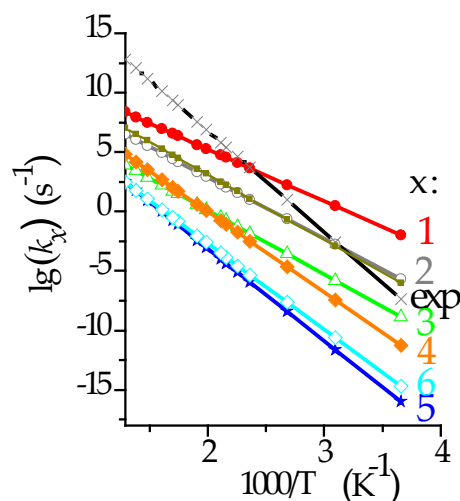


**Figure 6.** Rate constants ( $k_x$ ) for  $\text{DMO}^+$  methylation ( $x = 1\text{--}4$ ) and  $\text{DMO}^+$  H-abstraction ( $x = 5\text{--}6$ ), and the experimental synthesis of methyl acetate ( $k_{\text{exp}}$ ).

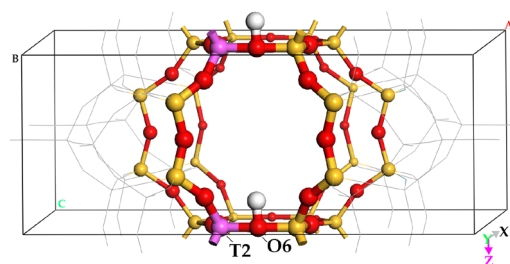
As calculated, the rate constants at 463.15 K for six designed reactions (Equations (1)–(6)) are about  $3.4 \times 10^4$ ,  $1.1 \times 10^2$ , 0.18,  $8.2 \times 10^{-2}$ ,  $4.4 \times 10^{-5}$ , and  $1.4 \times 10^{-4} \text{ s}^{-1}$ , respectively. Those numerical values of rate constants imply that  $\text{DMO}^+$  and  $\text{TMO}^+$  are likely to be produced in DME carbonylation. Both  $\text{DMO}^+$  and  $\text{TMO}^+$  act as sources of the methyl agent and are more likely to take part in the sequent CO insertion steps [1,2,6,7,16]. It is worth noting that the orientation of the attacking molecules and the stereoscopic effect will have some influences on the chemical reaction.

### 3. Materials and Methods

All calculations are carried out using the Vienna Ab initio Simulation Package (VASP) [59–62] implemented with the plane-wave periodic gradient-corrected density functional theory methods. The Perdew–Burke–Ernzerh (PBE) [63] pseudopotentials (version 52) are used to describe the exchange–correlation functional, and the projector augmented wave approximation (PAW) [64] of Blöchl is adopted to describe the electron-ion interaction. Standard PAW pseudopotentials are used in this study. The atoms involved are H, O, C, Al, and Si, and their ENMAX values are 250.00, 400.00, 400.00, 240.30, and 245.35 eV, respectively. The kinetic energy cut-off for the plane wave basis is set to 570.00 eV, which is about 42.5% higher than the maximum of ENMAX (400.00 eV) of all atoms involved. The K-mesh of  $1 \times 1 \times 1$  is used to describe the Brillouin zone sampling. A quasi-Newton algorithm is used to relax the ions. The self-consistency loop will break, and the structural energy minimization will stop when both the total energy change and the band structure energy change between two iteration steps are smaller than  $1.0 \times 10^{-7} \text{ eV}$  per atom; the ionic relaxation will not be updated if all forces on all atoms are less than  $1.0 \times 10^{-2} \text{ eV/\AA}$ . These calculation parameters have been tested. The total energy of species is almost unchangeable with increasing cutoff energy (Figure S2 in Supplementary Materials). If the K-mesh of H-FER increases to  $2 \times 2 \times 2$ , the calculated activated internal energy changes slightly within  $\pm 1.00 \text{ kcal/mol}$ , and the reaction heat changes slightly within  $\pm 2.00 \text{ kcal/mol}$  (Table S1 in Supplementary Materials); however, the calculation is not easy to converge and the calculation time grows rapidly, and then the calculation becomes somewhat exhausting, and the expensive computational resource is a bit unbearable.

Taking the frequency analysis of TS6 computed in a node of Dell-R630 for an example, the calculation time is about 434,713.13 s when the K-mesh is  $1 \times 1 \times 1$ , but the calculation time is about 3.80 times as long as the K-mesh of  $1 \times 1 \times 1$  when the K-mesh becomes  $2 \times 2 \times 2$ . Herein, the computational node of Dell-R630 is from Shandong University (Qingdao Campus), each node has two CPUs of Intel® Xeon® E5-2670 v3 and 64 GB memory capacity and each CPU has 2 sockets and 12 cores/package. Therefore, the selection of calculation parameters in this study could be ascribed to the tradeoff between calculation precision and computation efficiency.

A structure model with a Si/Al ratio of 35:1 is selected to represent the topology of the acidic zeolite ferrierite, denoted as H-FER. In this model, one unit cell of H-FER contains 1 Al atom, 36 Si atoms, 72 O atoms, 1 hydrogen atom, and 1 fer cage (Scheme 2). The unit cell of H-FER is a variant of a standard unit cell of the pure silica FER framework. The H-FER unit cell is derived from the pure silicon FER framework by introducing an isomorphous Si  $\rightarrow$  Al substitution at the T2 site. To maintain charge neutrality, a hydrogen atom is introduced to the framework O6 position. In fact, this specific configuration is one of the Brønsted acid sites of the acidic zeolite ferrierite called T2O6. The pure silicon FER framework with the space group of Immm is initially obtained from the Database of Zeolite Structures in the internal zeolite associates (IZA) [65].



**Scheme 2.** A fer cage (highlights in ball and stick) within the T2O6 configuration of the acidic zeolite ferrierite (H-FER). Note that grey lines stand for interconnecting atoms and bonds away from the fer cage.

Through the standard prediction procedure [66–68], the unit cell volume of H-FER at the T2O6 site could be obtained through the E(V) curve (Figure S3 in Supplementary Materials) fitting with the Birch-Murnaghan equation and the following calculation of the full geometry optimization. Herein, the E(V) curve is obtained through a series of single-point energy calculations at some given volumes (ranging from 1900–2360 Å<sup>3</sup>) with an interval of 20 Å<sup>3</sup>; the full optimization of H-FER at the T2O6 site is carried out by relaxing the cell shape and the fractional coordinates. The calculated lattice parameters are  $a = 18.982$  Å,  $b = 14.324$  Å,  $c = 7.541$  Å, and  $V = 2050.526$  Å<sup>3</sup>. The calculated unit cell volume of H-FER at the T2O6 site slightly (i.e., 30.657 Å<sup>3</sup>) deviates from the experimental equilibrium volume of zeolite ferrierite [27,28]. When small attacking molecules (i.e., DME, CH<sub>3</sub>OH, H<sub>2</sub>O, and CO) are involved, the geometry optimization is performed by fixing the cell shape of H-FER at T2O6 and relaxing the fractional coordinates.

The second derivatives (Hessian matrix and phonon frequencies) are calculated using the density functional perturbation theory (DFPT). Besides the 3N-3 positive frequencies, each stable species (i.e., reactant, intermediate, or produce) still has three small imaginary frequencies ( $<6.49$   $i$  cm<sup>-1</sup>), although many efforts have been made to remove them. Each transition state has 3N-4 positive vibrations, one big main imaginary frequency, and three small imaginary frequencies ( $<5.80$   $i$  cm<sup>-1</sup>). Herein, N represents the total atom number of species in the computation model. Each of the small imaginary frequencies shows that the associated atoms oscillate nearly along one direction. It is reasonable to regard the associated nuclear motions as the translation/rotations of the species. The entropy contribution from those pseudo-translation/rotation degrees of freedom is almost equal to that from a harmonic vibration of 12 cm<sup>-1</sup> [67,69–71]. To reduce the computation error

as much as possible, three small imaginary frequencies would be replaced by a harmonic vibration of  $12\text{ cm}^{-1}$  during the entropy contribution calculation. The transition state is further verified as the desirable state to connect two stable species through vibrational analysis. The charges on atoms of each species are analyzed by the Bader charge method developed by the Henkelman group [72], on the basis of the fully optimized geometry. The optimized geometry of the transition state is verified as the minima along the reaction coordinate by vibrational analysis.

#### 4. Conclusions

The acidic zeolite ferrierite is one of the most effective halide-free catalysts to facilitate the fast conversion of DME to methyl acetate with high catalytic performances. DME undergoes a reaction with Brønsted acid proton to yield a dimethyl oxonium ion  $\text{DMO}^+$  (or  $(\text{CH}_3)_2\text{OH}^+$ ), also known as the protonated DME [48]. Six  $\text{DMO}^+$ -mediated reactions (Equations (1)–(6) are designed, which are classified into  $\text{DMO}^+$  methylation and  $\text{DMO}^+$  H-abstraction. The probability of those reactions has been further analyzed by using PDFT, statistical thermodynamics, the transition state theory, and the Bader decomposition of charge. Detailed information has been provided in this study, such as the adsorption complex, the reaction course, the structural parameter, the energy parameter, the product species, the Bader charge, and the rate constant.

In view of the [001] plane, the fer cage of zeolite ferrierite is a bit like the abdomen of a person (Figures 2 and 5). Within a fer cage, the courses for the reactions between the hydrogen-bonded DME and the attacking molecules are hypothesized to unfold as follows: (i) Initially, a DME molecule within the fer cage is expected to preferentially adsorb at T2O6 site perpendicular to the [010] plane of zeolite ferrierite; (ii) The Brønsted acid proton exhibits a strong tendency to transfer to the O atom of DME; (iii) Subsequently, the breakage of O-C bond of  $\text{DMO}^+$  take place, affording  $\text{CH}_3\text{OH}$  and a nearly planar intermediate species known as methyl cation ( $\text{CH}_3^+$ ); (iv) This methyl cation tends to transfer to O or C atom of the attacking molecules or to abstract one of methyl H atoms from DME or  $\text{CH}_3\text{OH}$ ; (v) The reactions involve the  $\text{S}_{\text{N}}2$ -like transition states in either  $\text{DMO}^+$  methylation or  $\text{DMO}^+$  H-abstraction; (vi) Various highly active intermediates are produced, such as  $(\text{CH}_3)_3\text{O}^+$ ,  $(\text{CH}_3)_2\text{OH}^+$ ,  $\text{CH}_3\text{CO}^+$ ,  $\text{CH}_3\text{OH}_2^+$ , and  $\text{CH}_2=\text{OH}^+$ , contributing to the complexity and the diversity of the reaction pathways within a fer cage.

According to our study, there are some convincing pieces of evidence to support the hypothesis that  $\text{DMO}^+$  is a highly active intermediate, and six  $\text{DMO}^+$ -mediated reactions are likely to occur at the optimized temperature range for DME carbonylation, running parallel to SMS-mediated reactions. (i)  $\text{DMO}^+$  has been observed in the IR spectra experiment [1,2,46]. (ii) As far as the activation internal energy is concerned, either  $\text{DMO}^+$  methylation or  $\text{DMO}^+$  H-abstraction is less than the experimental synthesis of methyl acetate [1,2], the barrier difference is 9.81–21.40 or 3.24–5.87 kcal/mol. (iii) At 463.15 K, the rate constants for Equations (1)–(6) are not too low, which are estimated to be about  $3.4 \times 10^4$ ,  $1.1 \times 10^2$ , 0.18,  $8.2 \times 10^{-2}$ ,  $4.4 \times 10^{-5}$ , and  $1.4 \times 10^{-4}\text{ s}^{-1}$ , respectively. Whether the reaction orientation is suitable,  $\text{DMO}^+$  is likely to act like the surface methoxyl species and then trigger and further propagate the sequent chemical reaction [1,2,6,7,12]. It is worth noting that the numerical values of energies, rate constants, charges, bond lengths, and bond angles are more or less influenced by the selected calculation parameter. The calculation parameter used in this study is based on a tradeoff between calculation precision and computational efficiency.

**Supplementary Materials:** The following supporting information can be downloaded at <https://www.mdpi.com/article/10.3390/molecules29092000/s1>. Figure S1: The pore sizes of (a) 8- and (b) 10-member channels of zeolites ferrierite and (c) the molecule size of dimethyl ether (DME); Figure S2: Total energy of zeolite ferrierite dependent on the energy cutoff; Figure S3: Total energy of zeolite ferrierite dependent on the unit cell volume; Figure S4: Schematic structures of reactants (Rex), transition states (TSx), and products (Px) from Equation (x) (x = 1–6). For Equation (x), please refer to the Section 1; Table S1: The energy difference (in kcal/mol) between two types of K-meshes

(i.e.,  $1 \times 1 \times 1$  and  $2 \times 2 \times 2$ ) of H-FER; Table S2: The fractional coordinates for Rex, TSx, and Px from Equation (x) ( $x = 1-6$ ).

**Author Contributions:** X.C.: Conceptualization, methodology, software, validation, formal analysis, investigation, resources, data curation, writing—original draft preparation, writing—review and editing, visualization, supervision, project administration, funding acquisition. P.F.: investigation. X.L.: validation, writing—review and editing, and funding acquisition. All authors have read and agreed to the published version of the manuscript.

**Funding:** This research was funded by the Fundamental Research Funds (No. 2019GN018) of Shandong University, the Ministry of Science and Technology of China (Grant 2017YFA0204800), and the National Natural Science Foundation of China (Grant No. 22172162).

**Informed Consent Statement:** Not applicable.

**Data Availability Statement:** Data are contained within the article and Supplementary Materials.

**Acknowledgments:** We express great thanks to the support of Shandong University, the Dalian Institute of Chemical Physics, the National Natural Science Foundation of China, and the Ministry of Science and Technology of China. We also thank Yingxu Wei for the helpful discussion.

**Conflicts of Interest:** The authors declare no conflicts of interest.

## Abbreviations

BA	Brönsted acid;
MA	methyl acetate;
H-FER	the acidic zeolite ferrierite;
SMS or ZO-CH <sub>3</sub>	surface methoxy species on zeolites;
DME	dimethyl ether;
DMO <sup>+</sup>	dimethyl oxonium ion;
TMO <sup>+</sup>	trimethyl oxonium ion;
CH <sub>3</sub> OH <sub>2</sub> <sup>+</sup>	methoxonium ion;
$\Delta E^\ddagger$	the activation of internal energy.

## References

1. Cheung, P.; Bhan, A.; Sunley, G.J.; Iglesia, E. Selective Carbonylation of Dimethyl Ether to Methyl Acetate Catalyzed by Acidic Zeolites. *Angew. Chem. Int. Ed.* **2006**, *45*, 1617–1620. [[CrossRef](#)] [[PubMed](#)]
2. Cheung, P.; Bhan, A.; Sunley, G.J.; Law, D.J.; Iglesia, E. Site requirements and elementary steps in dimethyl ether carbonylation catalyzed by acidic zeolites. *J. Catal.* **2007**, *245*, 110–123. [[CrossRef](#)]
3. Bhan, A.; Allian, A.D.; Sunley, G.J.; Law, D.J.; Iglesia, E. Specificity of sites within eight-membered ring zeolite channels for carbonylation of methyls to acetyls. *J. Am. Chem. Soc.* **2007**, *129*, 4919–4924. [[CrossRef](#)] [[PubMed](#)]
4. Liu, J.; Xue, H.; Huang, X.; Li, Y.; Shen, W. Dimethyl Ether Carbonylation to Methyl Acetate over HZSM-35. *Catal. Lett.* **2010**, *139*, 33–37. [[CrossRef](#)]
5. Li, X.; Liu, X.; Liu, S.; Xie, S.; Zhu, X.; Chen, F.; Xu, L. Activity Enhancement of ZSM-35 in Dimethyl Ether Carbonylation Reaction through Alkaline Modifications. *RSC Adv.* **2013**, *3*, 16549–16557. [[CrossRef](#)]
6. Boronat, M.; Martínez-Sánchez, C.; Law, D.; Corma, A. Enzyme-like Specificity in Zeolites: A Unique Site Position in Mordenite for Selective Carbonylation of Methanol and Dimethyl Ether with CO. *J. Am. Chem. Soc.* **2008**, *130*, 16316–16323. [[CrossRef](#)] [[PubMed](#)]
7. Boronat, M.; Martínez, C.; Corma, A. Mechanistic differences between methanol and dimethyl ether carbonylation in side pockets and large channels of mordenite. *Phys. Chem. Chem. Phys.* **2011**, *13*, 2603–2612. [[CrossRef](#)] [[PubMed](#)]
8. Wang, S.; Guo, W.; Zhu, L.; Wang, H.; Qiu, K.; Cen, K. Methyl Acetate Synthesis from Dimethyl Ether Carbonylation over Mordenite Modified by Cation Exchange. *J. Phys. Chem. C* **2015**, *119*, 524–533. [[CrossRef](#)]
9. He, T.; Liu, X.; Xu, S.; Han, X.; Pan, X.; Hou, G.; Bao, X. Role of 12-Ring Channels of Mordenite in DME Carbonylation Investigated by Solid-State NMR. *J. Phys. Chem. C* **2016**, *120*, 22526–22531. [[CrossRef](#)]
10. Park, S.Y.; Shin, C.-H.; Bae, J.W. Selective carbonylation of dimethyl ether to methyl acetate on Ferrierite. *Catal. Commun.* **2016**, *75*, 28–31. [[CrossRef](#)]
11. Feng, P.; Chen, X.-F.; Li, X.-J.; Zhao, D.; Xie, S.J.; Xu, L.-Y.; He, G.-Z. The distribution analysis on the proton siting and the acid strength of the zeolite ferrierite: A computational study. *Microporous Mesoporous Mater.* **2017**, *239*, 354–362. [[CrossRef](#)]
12. Feng, P.; Zhang, G.; Zang, K.; Li, X.; Xu, L.; Chen, X. A theoretical study on the selective adsorption behavior of dimethyl ether and carbon monoxide on H-FER zeolites. *Chem. Phys. Lett.* **2017**, *684*, 279–284. [[CrossRef](#)]

13. Feng, P.; Zhang, G.; Chen, X.; Zang, K.; Li, X.; Xu, L. Specific zone within 8-membered ring channel as catalytic center for carbonylation of dimethyl ether and methanol over FER zeolite. *Appl. Catal. A Gen.* **2018**, *557*, 119–124. [[CrossRef](#)]
14. Li, L.; Wang, Q.; Liu, H.; Sun, T.; Fan, D.; Yang, M.; Tian, P.; Liu, Z. Preparation of Spherical Morденite Zeolite Assemblies with Excellent Catalytic Performance for Dimethyl Ether Carbonylation. *ACS Appl. Mater. Interfaces* **2018**, *10*, 32239–32246. [[CrossRef](#)] [[PubMed](#)]
15. Feng, X.; Yao, J.; Li, H.; Fang, Y.; Yoneyama, Y.; Yang, G. A brand new zeolite catalyst for carbonylation reaction. *Chem. Commun.* **2019**, *55*, 1048–1051. [[CrossRef](#)] [[PubMed](#)]
16. Zhan, E.; Xiong, Z.; Shen, W. Dimethyl ether carbonylation over zeolites. *J. Energy Chem.* **2019**, *36*, 51–63. [[CrossRef](#)]
17. Liua, S.; Fang, X.; Liu, Y.; Liu, H.; Ma, X.; Zhu, W.; Liu, Z. Dimethyl ether Carbonylation over Morденite zeolite modified by Alkylimidazolium ions. *Catal. Commun.* **2020**, *147*, 106161. [[CrossRef](#)]
18. Liu, S.; Liu, H.; Ma, X.; Yong, L.; Zhu, W.; Liu, Z. Identifying and controlling the acid site distributions in mordenite zeolite for dimethyl ether carbonylation reaction by means of selective ion-exchange. *Catal. Sci. Technol.* **2020**, *10*, 4663–4672. [[CrossRef](#)]
19. Li, S.; Cai, K.; Li, Y.; Liu, S.; Yu, M.; Wang, Y.; Ma, X.; Huang, S. Identifying the Active Silver Species in Carbonylation of Dimethyl Ether over Ag-HMOR. *ChemCatChem* **2020**, *12*, 3290–3297. [[CrossRef](#)]
20. Xiong, Z.; Zhan, E.; Li, M.; Shen, W. DME carbonylation over a HSUZ-4 zeolite. *Chem. Commun.* **2020**, *56*, 3401–3404. [[CrossRef](#)]
21. Kipnis, M.A.; Volnina, E.A. Methyl Acetate Synthesis by Dimethyl Ether Carbonylation in the Presence of Zeolites: A Review. *Kinet. Catal.* **2022**, *63*, 129–140. [[CrossRef](#)]
22. Fan, B.; Zhang, W.; Gao, P.; Hou, G.; Liu, R.; Xu, S.; Wei, Y.; Liu, Z. Quantitatively Mapping the Distribution of Intrinsic Acid Sites in Morденite Zeolite by High-Field  $^{23}\text{Na}$  Solid-State Nuclear Magnetic Resonance. *J. Phys. Chem. Lett.* **2022**, *13*, 5186–5194. [[CrossRef](#)] [[PubMed](#)]
23. Yao, J.; Feng, X.; Fan, J.; Komiyama, S.; Kugue, Y.; Guo, X.; He, Y.; Yang, G.; Tsubaki, N. Self-Assembled Nano-Filamentous Zeolite Catalyst to Realize Efficient One-Step Ethanol Synthesis. *Chem. A Eur. J* **2022**, *28*, e202201783. [[CrossRef](#)] [[PubMed](#)]
24. Feng, X.-B.; Cao, J.-P.; Su, C.; He, Z.-M.; Zhao, X.-Y. Tailoring the acid distribution and identifying the active center of rod-shaped HSUZ-4 zeolite for enhancing dimethyl ether carbonylation performance. *Fuel* **2022**, *315*, 123267. [[CrossRef](#)]
25. Xu, H.; Zhu, J.; Zhu, L.; Zhou, E.; Shen, C. Advances in the Synthesis of Ferrierite Zeolite. *Molecules* **2020**, *25*, 3722. [[CrossRef](#)]
26. Vaughan, P.A. crystal structures of zeolite ferrierite. *Am. Miner.* **1965**, *50*, 293–294. [[CrossRef](#)]
27. Kerr, I.S. Structure of Ferrierite. *Nature* **1966**, *210*, 294–295. [[CrossRef](#)]
28. Vaughan, P.A. The Crystal Structure of the Zeolite Ferrierite. *Acta. Crystallogr.* **1966**, *21*, 983–990. [[CrossRef](#)]
29. Morris, R.E.; Weigel, S.J.; Henson, N.J.; Bull, L.M.; Janicke, M.T.; Chmelka, B.F.; Cheetham, A.K. A Synchrotron X-ray Diffraction, Neutron Diffraction,  $^{29}\text{Si}$  MAS-NMR, and Computational Study of the Siliceous Form of Zeolite Ferrierite. *J. Am. Chem. Soc.* **1994**, *116*, 11849–11855. [[CrossRef](#)]
30. Blanco, F.; Urbinavillalba, G.; Deagudelo, M.M.R. Theoretical calculations on zeolites—The aluminum substitution in mordenite, ferrierite and ZSM-5. *Mol. Simul.* **1995**, *14*, 165–176. [[CrossRef](#)]
31. Dědeček, J.; Sobalík, Z.; Wichterlová, B. Siting and Distribution of Framework Aluminium Atoms in Silicon-Rich Zeolites and Impact on Catalysis. *Cat. Rev. Sci. Eng.* **2012**, *54*, 135–223. [[CrossRef](#)]
32. Xiong, Z.; Qi, G.; Bai, L.; Zhan, E.; Chu, Y.; Xu, J.; Ta, N.; Hao, A.; Deng, F.; Shen, W. Preferential population of Al atoms at the T4 site of ZSM-35 for the carbonylation of dimethyl ether. *Catal. Sci. Technol.* **2022**, *12*, 4993–4997. [[CrossRef](#)]
33. Martucci, A.; Alberti, A.; Cruciani, G.; Radaelli, P.; Ciambelli, P.; Rapacciuolo, M. Location of Brønsted sites in D-ferrierite by neutron powder diffraction. *Microporous Mesoporous Mater.* **1999**, *30*, 95–101. [[CrossRef](#)]
34. van Santen, R.A.; Kramer, G.J. Reactivity Theory of Zeolitic Brønsted Acidic Sites. *Chem. Rev.* **1995**, *95*, 637–660. [[CrossRef](#)]
35. Petersen, H.; Weidenthaler, C. A review of recent developments for the in situ/operando characterization of nanoporous materials. *Inorg. Chem. Front.* **2022**, *9*, 4244–4271. [[CrossRef](#)]
36. Bhan, A.; Iglesia, E. A Link between Reactivity and Local Structure in Acid Catalysis on Zeolites. *Acc. Chem. Res.* **2008**, *41*, 559–567. [[CrossRef](#)]
37. Voleska, I.; Nachtigall, P.; Ivanova, E.; Hadjiivanov, K.; Bulánek, R. Theoretical and experimental study of CO adsorption on Ca-FER zeolite. *Catal. Today* **2015**, *243*, 53–61. [[CrossRef](#)]
38. Catizzone, E.; Aloise, A.; Migliori, M.; Giordano, G. The effect of FER zeolite acid sites in methanol-to-dimethyl-ether catalytic dehydration. *J. Energy. Chem.* **2017**, *26*, 406–415. [[CrossRef](#)]
39. Xu, F.; Hong, Z.; Lv, J.; Chen, C.; Zhao, G.; Miao, L.; Yang, W.; Zhu, Z. Mg enhances the catalytic selectivity and stability of mordenite for carbonylation of dimethyl ether. *Appl. Catal. A Gen.* **2022**, *648*, 118928. [[CrossRef](#)]
40. Nachtigall, P.; Bulánek, R. Theoretical investigation of site-specific characteristics of CO adsorption complexes in the Li<sup>+</sup>-FER zeolite. *Appl. Catal. A Gen* **2006**, *307*, 118–127. [[CrossRef](#)]
41. Chu, Y.; Lo, A.-Y.; Wang, C.; Deng, F. Origin of High Selectivity of Dimethyl Ether Carbonylation in the 8-Membered Ring Channel of Morденite Zeolite. *J. Phys. Chem. C* **2019**, *123*, 15503–15512. [[CrossRef](#)]
42. Bordiga, S.; Palomino, G.T.; Paze, C.; Zecchina, A. Vibrational spectroscopy of H<sub>2</sub>, N<sub>2</sub>, CO and NO adsorbed on H, Li, Na, K-exchanged ferrierite. *Microporous Mesoporous Mater.* **2000**, *34*, 67–80. [[CrossRef](#)]
43. Cairon, O. CO adsorption on the Na, K-Ferrierite zeolite at 77 K and 193 K: New IR insights and consequences on the previously endorsed assignments of adsorbed species. *Microporous Mesoporous Mater.* **2014**, *183*, 48–53. [[CrossRef](#)]

44. van Well, W.J.M.; Cottin, X.; Smit, B.; van Hooff, J.H.C.; van Santen, R.A. Chain Length Effects of Linear Alkanes in Zeolite Ferrierite. 2. Molecular Simulations. *J. Phys. Chem. B* **1998**, *102*, 3952–3958. [[CrossRef](#)]
45. Rasmussen, D.B.; Christensen, J.M.; Temel, B.; Studt, F.; Moses, P.G.; Rossmesl, J.; Riisager, A.; Jensen, A.D. Ketene as a Reaction Intermediate in the Carbonylation of Dimethyl Ether to Methyl Acetate over Mordenite. *Angew. Chem.* **2015**, *127*, 7369–7372. [[CrossRef](#)]
46. Forester, T.R.; Howe, R.F. In Situ FTIR Studies of Methanol and Dimethyl Ether in ZSM-5. *J. Am. Chem. Soc.* **1987**, *109*, 5076–5082. [[CrossRef](#)]
47. Zicovich-Wilson, C.M.; Viruela, P.; Corma, A. Formation of Surface Methoxy Groups on H-Zeolites from Methanol. A Quantum Chemical Study. *J. Phys. Chem.* **1995**, *99*, 13224–13231. [[CrossRef](#)]
48. Olah, G.A.; Burcher, A.; Rasul, G.; Gnann, R.; Christe, K.O.; Prakash, G.K.S. <sup>17</sup>O and <sup>13</sup>C NMR/ab Initio/IGLO/GIAO-MP2 Study of Oxonium and Carboxonium Ions (Dications) and Comparison with Experimental Data. *J. Am. Chem. Soc.* **1997**, *119*, 8035–8042. [[CrossRef](#)]
49. Fang, H.; Zheng, A.; Chu, Y.; Deng, F. <sup>13</sup>C Chemical Shift of Adsorbed Acetone for Measuring the Acid Strength of Solid Acids: A Theoretical Calculation Study. *J. Phys. Chem. C* **2010**, *114*, 12711–12718. [[CrossRef](#)]
50. Olah, G.A.; Prakash, G.K.S.; Ellis, R.W.; Olah, J.A. Remarks on the Mechanism of Ethylene Formation from Methyl Alcohol. *J. Chem. Soc. Chem. Commun.* **1986**, 9–10. [[CrossRef](#)]
51. Olah, G.A.; Doggweiler, H.; Felberg, J.D. Onium Ylide chemistry. 2. Methylenealkyloxonium Ylides. *J. Org. Chem.* **1984**, *49*, 2116–2122. [[CrossRef](#)]
52. Poreddy, R.; Mossin, S.; Jensen, A.D.; Riisager, A. Promoting Effect of Copper Loading and Mesoporosity on Cu-MOR in the Carbonylation of Dimethyl Ether to Methyl Acetate. *Catalysts* **2021**, *11*, 696. [[CrossRef](#)]
53. Olah, G.A.; Mathew, T.; Prakash, G.K.S.; Rasul, G. Chemical Aspects of Astrophysically Observed Extraterrestrial Methanol, Hydrocarbon Derivatives, and Ions. *J. Am. Chem. Soc.* **2016**, *138*, 1717–1722. [[CrossRef](#)] [[PubMed](#)]
54. Li, J.; Wei, Z.; Chen, Y.; Jing, B.; He, Y.; Dong, M.; Jiao, H.; Li, X.; Qin, Z.; Wang, J.; et al. A route to form initial hydrocarbon pool species in methanol conversion to olefins over zeolites. *J. Catal.* **2014**, *317*, 277–283. [[CrossRef](#)]
55. Wei, Z.; Chen, Y.-Y.; Li, J.; Guo, W.; Wang, S.; Dong, M.; Qin, Z.; Wang, J.; Jiao, H.; Fan, W. Stability and Reactivity of Intermediates of Methanol Related Reactions and C-C Bond Formation over H-ZSM-5 Acidic Catalyst: A Computational Analysis. *J. Phys. Chem. C* **2016**, *120*, 6075–6087. [[CrossRef](#)]
56. Svelle, S.; Visur, M.; Olsbye, U.; Saepurahman; Bjørgen, M. Mechanistic Aspects of the Zeolite Catalyzed Methylation of Alkenes and Aromatics with Methanol: A Review. *Top. Catal.* **2011**, *54*, 897–906. [[CrossRef](#)]
57. Olah, G.A.; Doggweiler, H.; Felberg, J.D.; Frohlich, S.; Grdina, M.J.; Karpeles, R.; Keumi, T.; Inaba, S.-i.; Lammertsma, W.M.I.K.; Salem, G.; et al. Onium Ylide Chemistry. 1. Bifunctional Acid-Base-Catalyzed Conversion of Heterosubstituted Methanes into Ethylene and Derived Hydrocarbons. The Onium Ylide Mechanism of the C<sub>1</sub>→C<sub>2</sub> conversion. *J. Am. Chem. Soc.* **1984**, *106*, 2143–2149. [[CrossRef](#)]
58. Olah, G.A.; Doggweiler, H.; Felberg, J.D.; Frohlich, S. Onium Ions. 33. (Trimethylsilyl)- and [(Trimethylsilyl)methyl]oxonium and -halonium Ions. *J. Org. Chem.* **1985**, *50*, 4847–4851. [[CrossRef](#)]
59. Kresse, G.; Hafner, J. Ab Initio Molecular Dynamics for Liquid Metals. *Phys. Rev. B* **1993**, *48*, 13115–13118. [[CrossRef](#)]
60. Kresse, G.; Hafner, J. Ab Initio Molecular-Dynamics Simulation of the Liquid-Metal Amorphous-Semiconductor Transition in Germanium. *Phys. Rev. B Condens. Matter. Mater. Phys.* **1994**, *49*, 14251–14269. [[CrossRef](#)]
61. Kresse, G.; Furthmüller, J. Efficiency of Ab-initio Total Energy Calculations for Metals and Semiconductors Using a Plane-Wave Basis Set. *Comput. Mat. Sci.* **1996**, *6*, 15–50. [[CrossRef](#)]
62. Kresse, G.; Furthmüller, J. Efficient Iterative Schemes for Ab Initio Total-energy Calculations Using a Plane-Wave Basis Set. *Phys. Rev. B* **1996**, *54*, 11169–11186. [[CrossRef](#)] [[PubMed](#)]
63. Perdew, J.P.; Burke, K.; Ernzerhof, M. Generalized Gradient Approximation Made Simple. *Phys. Rev. Lett.* **1996**, *77*, 3865–3868. [[CrossRef](#)] [[PubMed](#)]
64. Blöchl, P.E. Projector augmented-wave method. *Phys. Rev. B* **1994**, *50*, 17953–17979. [[CrossRef](#)] [[PubMed](#)]
65. Baerlocher, C.; McCusker, L.B. Database of Zeolite Structures. Available online: <http://www.iza-structure.org/databases> (accessed on 14 April 2024).
66. Grajciar, L.; Areán, C.O.; Pulido, A.; Nachtigall, P. Periodic DFT investigation of the effect of aluminium content on the properties of the acid zeolite H-FER. *Phys. Chem. Chem. Phys.* **2010**, *12*, 1497–1506. [[CrossRef](#)]
67. Chen, X.; Yu, T. Simulating Crystal Structure, Acidity, Proton Distribution, and IR Spectra of Acid Zeolite HSAPO-34: A High Accuracy Study. *Molecules* **2023**, *28*, 8087. [[CrossRef](#)] [[PubMed](#)]
68. Chen, X.-F. Periodic Density Functional Theory (PDFT) Simulating Crystal Structures with Microporous CHA Framework: An Accuracy and Efficiency Study. *Inorganics* **2023**, *11*, 215. [[CrossRef](#)]
69. Brogaard, R.Y.; Weckhuysen, B.M.; Nørskov, J.K. Guest–host interactions of arenes in H-ZSM-5 and their impact on methanol-to-hydrocarbons deactivation processes. *J. Catal.* **2013**, *300*, 235–241. [[CrossRef](#)]
70. Brogaard, R.Y.; Henry, R.; Schuurman, Y.; Medford, A.J.; Moses, P.G.; Beato, P.; Svelle, S.; Nørskov, J.K.; Olsbye, U. Methanol-to-hydrocarbons conversion: The alkene methylation pathway. *J. Catal.* **2014**, *314*, 159–169. [[CrossRef](#)]

71. Ghorbanpour, A.; Rimer, J.D.; Grabow, L.C. Computational Assessment of the Dominant Factors Governing the Mechanism of Methanol Dehydration over H-ZSM-5 with Heterogeneous Aluminum Distribution. *ACS Catal.* **2016**, *6*, 2287–2298. [[CrossRef](#)]
72. Henkelman, G.; Arnaldson, A.; Jopsson, H. A fast and robust algorithm for Bader decomposition of charge density. *Comput. Mater. Sci.* **2006**, *31*, 354–360. [[CrossRef](#)]

**Disclaimer/Publisher’s Note:** The statements, opinions and data contained in all publications are solely those of the individual author(s) and contributor(s) and not of MDPI and/or the editor(s). MDPI and/or the editor(s) disclaim responsibility for any injury to people or property resulting from any ideas, methods, instructions or products referred to in the content.